Research Article | Vol. 29, No. 24 / 22 Nov 2021 / Optics Express 40633
Optics EXPRESS

Conical third harmonic generation from volume nanogratings induced by filamentation of femtosecond pulses in transparent bulk materials

ROBERTAS GRIGUTIS,[1] VYTAUTAS JUKNA,[1] MARIUS NAVICKAS,[1] GINTARAS TAMOŠAUSKAS,[1] KESTUTIS STALIUNAS,[1,2,3] AND AUDRIUS DUBIETIS[1,*]

[1] *Laser Research Center, Vilnius University, Sauletekio Avenue 10, LT-10223 Vilnius, Lithuania*
[2] *Institució Catalana de Recerca i Estudis Avançats (ICREA), Passeig Lluís Companys 23, 08010 Barcelona, Catalonia, Spain*
[3] *Universitat Politècnica de Catalunya (UPC), Rambla Sant Nebridi 22, 08222 Terrassa (Barcelona), Spain*
[*] *audrius.dubietis@ff.vu.lt*

Abstract: We report on observations of conical third harmonic emission that emerges during supercontinuum generation produced by self-focusing and filamentation of high (20-200 kHz) repetition rate 180 fs, 1035 nm pulses from an amplified Yb:KGW laser in various nonlinear crystals and glasses: YAG, sapphire, YLF, LiF, CaF_2, MgF_2, LiSAF, fused silica and BK-7 glass. We show that conical third harmonic generation is a phase-matched four-wave mixing process, where noncollinear phase matching is achieved by means of reciprocal lattice vector, inversely proportional to the period of nanograting, which is inscribed by femtosecond filament in the volume of nonlinear material. The existence of a particular period required to phase match conical third harmonic generation was indirectly verified by investigations of periodicity features of high and low spatial frequency laser-induced periodic surface structures, in which matter is reorganized in a similar fashion.

1. Introduction

Laser-induced periodic surface structures (LIPSS) represent an universal phenomenon and occur on almost every inorganic solid, including metals, semiconductors and dielectrics, under irradiation of continuous wave [1] or pulsed [2] laser operation regimes at various wavelengths [3,4]. LIPSS are produced within the focal spot of the linearly polarized laser beam. Typically, these structures emerge as a (quasi-)periodic surface relief modulation and feature a structural size from several micrometers down to less than 100 nm [5]. Spatial LIPSS characteristics (period, orientation) can be controlled by the irradiation geometry, laser wavelength, polarization state, peak fluence, and the number of pulses applied to the irradiated area [6–13]. LIPSS are fabricated in a single-step process and attract a great scientific and technological interest inspired by expanding applications in many areas of modern science, where easy and robust tailoring of mechanical, optical, or chemical properties of the material is of demand, in particular concerning the applications in plasmonics, photonics, microfluidics, medicine, and tribology [14–18].

During the past two decades, remarkable efforts were made to explain the origin of LIPSS formation, whether LIPSS are seeded via ultrafast electromagnetic energy scattering and absorption effects during the laser irradiation (electromagnetic interference model), or matter reorganization effects that occur after the irradiation process (matter self-organization model). Currently, both theories have been joined into a single more generalized approach, which states that during the LIPSS formation, both, laser irradiation conditions and material properties determine which effect (electromagnetic or self-organization of matter) is dominating [19].

#444901 https://doi.org/10.1364/OE.444901
Journal © 2021 Received 30 Sep 2021; accepted 11 Nov 2021; published 19 Nov 2021

Optics EXPRESS

LIPSS are classified into two groups according to their spatial periods (Λ) and orientation with respect to the laser beam polarization [15]: common wavelength-sized low-spatial-frequency LIPSS (LSFL) with $\Lambda > \lambda/2$, which on metals are usually oriented perpendicular to the laser beam polarization, and high-spatial-frequency LIPSS (HSFL) with $\Lambda < \lambda/2$, which are exclusively observed after irradiation of solids by ultrashort laser pulses.

In dielectrics incubation phenomena play a significant role under irradiation by multiple ultrashort laser pulses, as they lead to transient and permanent electronic defect states, which act as precursors for LIPSS formation. LSFL with periods close to $\sim \lambda/n_0$, with n_0 being the refractive index of the material, are often observed. For narrow band gap dielectrics, as well as for semiconductors, LSFL orientation is usually perpendicular to the laser beam polarization direction. In contrast, for wide band gap dielectric materials, LSFL orientation is often parallel to the polarization. HSFL with periods between λ/n_0 and $\lambda/(2n_0)$ are typically observed at lower peak fluences and larger number of pulses. Regardless of the band gap energy, HSFL are predominantly oriented perpendicular to the laser polarization direction. Also, gradual transition from conventional LIPSS to a polarization-independent low spatial frequency annular structures (LIPASS) in the center of the damage crater was discovered in fused silica [20], and more recently reported in chalcogenide glass [21]. Formation of periodic sub-wavelength nanogratings in the volume of various transparent dielectric materials upon tight focusing of multiple ultrashort laser pulses was observed as well [22–28], suggesting very similar underlying physics of their formation with HSFL [14,29,30].

However, the nonlinear optical phenomena arising from ultrashort pulse propagation in these structures are much less investigated to date. Third harmonic generation and diffraction via interaction of the incident wave vectors and a grating vector was observed under various interaction geometries in photo-thermo refractive [31,32] and silica [33] glasses. In the regime of femtosecond filamentation, specific emission patterns of broadband light, termed ciliary white light, were discovered [34,35]. The formation mechanisms of ciliary white light were attributed either to the diffraction of the supercontinuum radiation on the damage crater covered by sub-micron structures [34] or to the interference of white light emissions from neighboring small-scale filaments formed due to refraction at the damage site [35]. More recently, conical third harmonic generation accompanying extinction of supercontinuum spectrum due to nanograting formation at the nonlinear focus of the beam was observed, suggesting that conical third harmonic generation is a clear signature of optical degradation of the nonlinear material that ends up with catastrophic optical damage in the bulk [36].

In this paper we performed a detailed study of conical third harmonic generation demonstrating that it occurs as phase matched four-wave mixing process, obeying noncollinear phase matching condition, which involves reciprocal lattice vector of a nanograting inscribed by a femtosecond filament. Since direct characterization of nanogratings in the volume is technically difficult, we first study the evolution of structure morphology and periodicity of LIPSS inscribed in various transparent dielectric materials and show that these structures possess very broad distributions of periods. In filament-induced nanogratings, the matter is reorganized in a similar fashion, providing similar distribution of periods, containing the particular period required to phase match conical third harmonic (TH) generation, which is experimentally demonstrated in YAG, sapphire, YLF, LiF, CaF_2, MgF_2, LiSAF, fused silica and BK-7 glass.

2. Laser-induced periodic surface structures

The experiments were performed using a commercial amplified femtosecond Yb:KGW laser (Pharos, Light Conversion) generating 180 fs pulses with a central wavelength of 1035 nm at a repetition rate up to 200 kHz. LIPSS formation was investigated in detail in sapphire (Al_2O_3), yttrium aluminum garnet (YAG), magnesium fluoride (MgF_2), calcium fluoride (CaF_2), and fused silica (SiO_2) by focusing linearly polarized laser beam with a $1/e^2$ diameter of 5.08 mm

Optics EXPRESS

onto the front face of the sample. The focusing conditions (the numerical aperture, NA=0.025) and energy density (fluence) were established experimentally, and laser repetition rate was 200 kHz for YAG and sapphire and 20 kHz for CaF_2, MgF_2 and fused silica, as in these materials LIPSS were inscribed much faster. The samples were mounted on a three-dimensional translation stage, which allowed translation of the samples to a "fresh" (unexposed) site after each series of laser irradiation performed by varying number of pulses and incident energy (fluence). The morphology of produced LIPSS was characterized by scanning electron microscope, SEM (Prisma E, Thermo Fisher Scientific). Finally, a two-dimensional Fourier-transform (2D-FT) of the respective SEM images was performed to determine the period of LIPSS.

First, we examined the morphology and periodicity of LIPSS in sapphire irradiated by different number of consecutive pulses with a peak fluence F = 4.2 J/cm^2 and laser repetition rate of 200 kHz. Figures 1(a)–1(c) show the representative LIPSS morphologies, which could be attributed to HSFL, LSFL and LIPASS, respectively. The SEM images demonstrate how LIPSS morphology varies as a function of number of laser shots (pulses). After 20 laser pulses, well-aligned HSFL (oriented perpendicular to the laser polarization direction) are formed at the irradiated area [Fig. 1(a)]. A slightly larger number of pulses (30) produces LSFL whose orientation is less

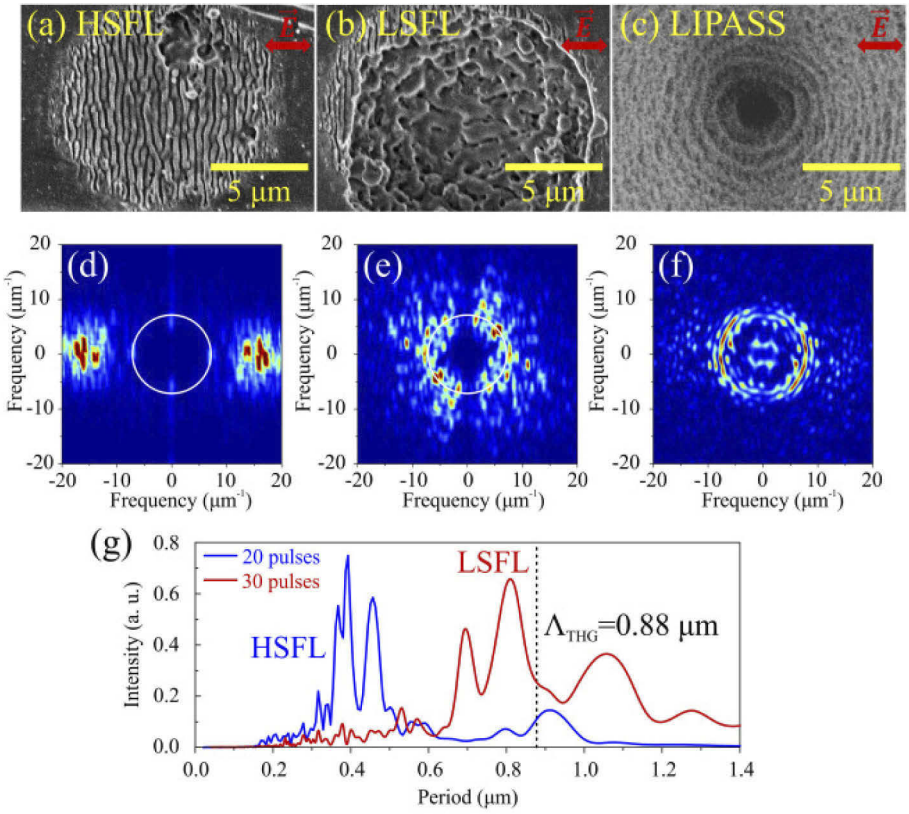

Fig. 1. SEM images showing LIPSS morphology of sapphire surface produced by femtosecond pulses with a peak fluence of 4.2 J/cm^2 and 200 kHz pulse repetition rate: (a) HSFL, produced with 20 laser pulses, (b) LSFL, 30 laser pulses, (c) LIPASS, 3×10^5 laser pulses. Arrows indicate the laser pulse polarization direction. (d), (e) and (f) present the corresponding Fourier spectra retrieved by 2D-FT of SEM images. White circles in (d) and (e) denote the spatial frequencies required to phase-match conical TH generation. (g) The distributions of periods in HSFL (blue curve) and LSFL (red curve).

Optics EXPRESS

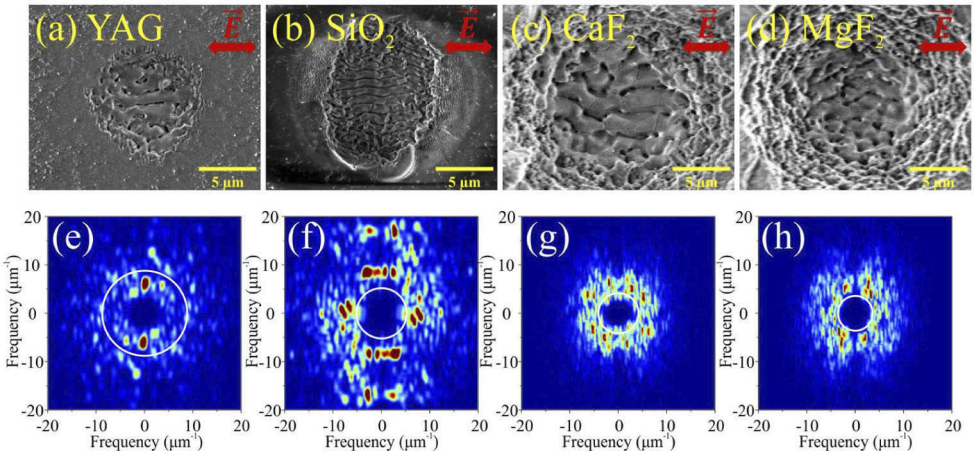

Fig. 2. SEM images of LSFL in (a) YAG produced with 10 pulses, F = 2.9 J/cm^2, (b) fused silica, 10 pulses, F = 4.2 J/cm^2, (c) CaF_2, 20 pulses, F = 4.9 J/cm^2, (d) MgF_2, 30 pulses, F = 4.9 J/cm^2. (e), (f), (g) and (h) show the corresponding 2D-FT data with white circles indicating the spatial frequencies that yield the required periods to phase-match conical TH generation.

defined [Fig. 1(b)]. Notice, that HSFL are still visible in the periphery, where the fluence of laser beam is lower. A further increase of number of pulses produces the damage crater, which gradually deepens, and the transition from traditional LIPSS to polarization-independent sub-wavelength annular structure, LIPASS, is observed, as shown in Fig. 1(c). Note, that the transition from HSFL to LSFL occurs on very fast time scale (just 10 additional laser pulses result in remarkable change of morphology), whereas the full development of LIPASS requires a considerable number of pulses (3×10^5).

Figures 1(d)–1(f) present the corresponding spatial frequency spectra retrieved by two-dimensional Fourier transform (2D-FT) of SEM images, showing that each particular LIPSS morphology contains a broad spectrum of spatial frequencies. More specifically, the transition from HSFL to LSFL reveals a remarkable change of Fourier spectrum towards smaller spatial frequencies, i.e., larger periods: $\Lambda \approx 320 - 500$ nm for HSFL and $\Lambda \approx 650 - 1200$ nm for LSFL. This change is shown in more detail in Fig. 1(g), which for the sake of clarity represents the distributions of periods retrieved from the central cross-sections of 2D-FT data shown in Figs. 1(d) and 1(e). 2D-FT performed on LIPASS [Fig. 1(f)] yielded spectrum of spatial frequencies, which converts into the interval of periods ranging from 630 to 1000 nm.

Very similar evolution of morphology from HSFL to LSFL and eventually to LIPASS, with increasing the number of pulses was observed in YAG, fused silica, CaF_2 and MgF_2, attesting the universal character of such morphological transition. Figure 2 presents SEM images of inscribed LSFL in YAG, fused silica, CaF_2 and MgF_2 and corresponding spatial frequency spectra retrieved by 2D-FT, showing that spatial frequencies are distributed over broad value ranges, which are slightly different for each particular material. Since during formation of nanogratings the matter is reorganized in a similar fashion as during inscription of LIPSS [14,29,30], we assume that filament-inscribed nanogratings possess broad distributions of periods similar to those present in HSFL and LSFL. Note that LIPASS represents a sole surface structure occurring due to interference between the incident laser field and the reflected light from damage crater walls [20], hence structures of this type are not related to nanograting formation in the bulk.

Optics EXPRESS

3. Experimental details

In order to disclose the intimate link between nanogratings and conical third harmonic generation, we conducted a series of experiments on supercontinuum generation in various nonlinear media, which beside the mentioned sapphire, YAG, CaF_2, MgF_2 and fused silica, include yttrium lithium fluoride (YLF), lithium fluoride (LiF), strontium hexafluoroaluminate (LiSAF) and borosilicate glass (BK-7). In these experiments the energy of the pump pulse (or the ratio between its peak power and critical power for self-focusing) for each particular material was set to produce a single filament which generates supercontinuum, while the focusing condition (the numerical aperture, NA) and laser repetition rate were set to observe extinction of supercontinuum radiation and occurrence of conical TH at reasonable exposure times. The energy and consequently the fluence of the pump pulse in these experiments was well below that produces surface structuring of the nonlinear material. Since sapphire and YAG exhibit the highest resistance to optical damage induced by repetitive laser pulses [36], in these materials we used tighter focusing of the pump beam (NA=0.051 and NA=0.085, respectively) and the highest available laser repetition rate (200 kHz). Supercontinuum generation in the rest materials was performed with NA=0.01 and laser repetition rate of 20 kHz; see Table 1, which provides a summary of the experimental parameters.

Table 1. Summary of experimental parameters: *f* is the laser pulse repetition rate, NA is the numerical aperture, *L* is the length of nonlinear material, E_p is the pump pulse energy, P/P_{cr} is the ratio of pump pulse peak power and critical power for self-focusing.

Material	f, kHz	NA	L, mm	E_p, μJ	P/P_{cr}
Sapphire	200	0.051	6	2.0	3.8
YAG	200	0.085	6	1.5	5.8
Fused silica	20	0.01	4.5	2.6	3.2
BK-7	20	0.01	10	2.6	5.2
CaF_2	20	0.01	5	3.5	2.3
MgF_2	20	0.01	4	3.9	1.7
LiF	20	0.01	3.5	5.9	2.3
YLF	20	0.01	5	2.4	2.1
LiSAF	20	0.01	5	4.8	1.2

Figure 3 presents examples of conical TH emission patterns in sapphire, BK-7 and LiF, which visually appear as distinct blue rings due to paper luminescence and partially extinguished supercontinuum that is generated on the propagation axis. The images were taken keeping identical aspect ratio as to highlight the differences in TH cone angles in different materials. It is important to mention, that no collinear (on the beam propagation axis, overlapping with supercontinuum) TH generation was observed in any of operating conditions: below and above filamentation and supercontinuum generation threshold, in the absence and in the presence of structural changes in the volume of material, i.e. material reorganization and formation of a nanograting. Whereas conical TH generation was observed only after a certain exposure time that in filamentation regime correlated with the extinction of supercontinuum, in line with earlier observations reported in [36]. Therefore we suppose that self-focusing and filamentation of high repetition rate femtosecond laser pulses inscribes a periodic structure (nanograting) in the volume of transparent nonlinear material, which contains a particular period, allowing to phase-match conical TH generation.

Optics EXPRESS

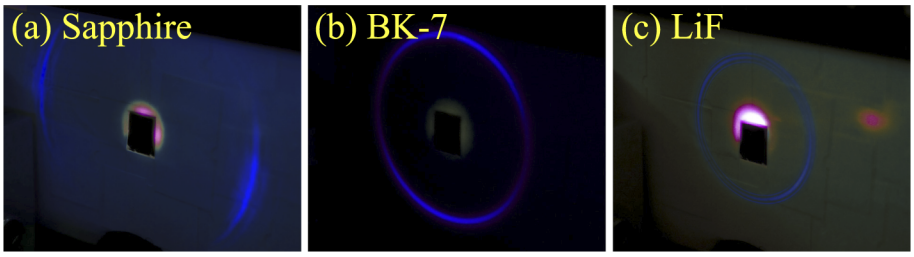

Fig. 3. Screenshots of conical TH emission during beam filamentation and supercontinuum generation in: (a) sapphire, (b) BK-7 and (c) LiF. The intense spots of supercontinuum emission in the center were blocked in order to ensure better visibility of conical TH.

4. Phase-matching considerations for conical TH generation

Conical TH generation is considered as a noncollinear phase-matched four-wave mixing process, as depicted in Fig. 4. The phase-matching condition for conical TH generation is a vector equation and reads as

$$3\mathbf{k_1} - \mathbf{k_3} + \mathbf{G} = \mathbf{0} \tag{1}$$

where $\mathbf{k_1}$ and $\mathbf{k_3}$ are the wave-vectors of the fundamental and TH waves, respectively, and $\mathbf{G}$ is the reciprocal lattice vector, inversely proportional to the nanograting period. The phase-matching equation, projected on directions parallel and perpendicular to the fundamental wave vector, becomes

$$\Delta k_{\parallel} = 3k_1 - k_3 \cos\alpha \tag{2}$$

and

$$\Delta k_{\perp} = k_3 \sin\alpha - G \tag{3}$$

where $k_1 = \omega_1 n_1/c$, $k_3 = \omega_3 n_3/c$, with n_1 and n_3 being the refractive indexes at fundamental (1035 nm) and TH (345 nm) wavelengths, respectively, and $G = 2\pi/\Lambda$, where Λ is the nanograting period. $\Delta k_{\parallel}$ and $\Delta k_{\perp}$ are the phase-mismatch parameters in the longitudinal and transverse directions, respectively, and to achieve phase-matching, both must vanish. Phase-matching in the longitudinal direction ($\Delta k_{\parallel} = 0$) gives the TH propagation angle (inside the material)

$$\alpha = \arccos\left(\frac{n_1}{n_3}\right), \tag{4}$$

while phase-matching in the transverse direction ($\Delta k_{\perp} = 0$) yields the nanograting period, which is expressed as

$$\Lambda = \frac{\lambda_3}{\sqrt{n_3^2 - n_1^2}}, \tag{5}$$

where λ_3 denotes the TH wavelength. Therefore, the values of both, TH cone angle and nanograting period, required for phase-matched conical TH generation, are solely determined by dispersive properties of the nonlinear material, through the refractive indexes n_1 and n_3. On the other hand, the transverse phase-matching involves the reciprocal lattice vector that is enabled via material reorganization yielding periodic modulation of, e.g. density [24] and refractive index [32,33], which lead to appropriate $\chi^{(3)}$ modulation.

Optics EXPRESS

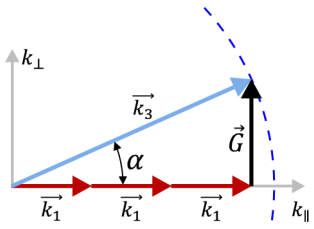

Fig. 4. Phase-matching diagram for conical TH generation.

5. Results and discussion

Experimentally, the TH cone angles in the air were measured by projecting the image on the paper screen located at known position from the crystal, as illustrated in Fig. 3. Thereafter the measured TH cone angles in the air were converted to internal angles (inside the medium) using Snell's law. The experimental data is summarized in Fig. 5(a), which plots the measured TH cone angles in all investigated materials as a function of n_1/n_3, attesting a fair agreement with the calculated TH cone angles using Eq. (4). The error bars to experimental points represent the angular widths of TH cones.

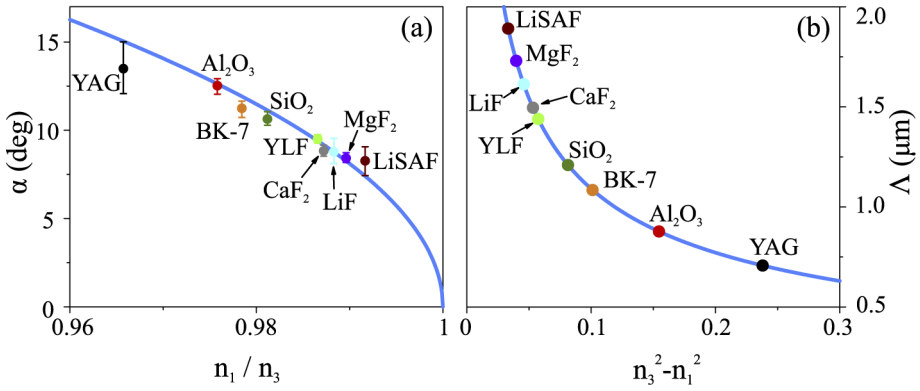

Fig. 5. (a) Measured (dots) and calculated (blue solid curve) internal TH cone angles. (b) Calculated nanograting periods required to phase-match conical TH generation. Bold dots mark the predicted values for investigated materials.

Figure 5(b) shows the calculated nanograting periods from Eq. (5) that provide reciprocal grating vectors of the required length to fulfill phase-matching condition for conical TH generation. The periods for investigated materials are indicated by bold dots. We assume that filament-induced nanogratings possess broad spectra of spatial frequencies (periods) that are distributed in a similar fashion as those extracted by 2D-FT analysis of LIPSS (HSFL and LSFL) presented in Section 2. Indeed, the markings of specific spatial frequencies and related periods of LIPSS in sapphire, see Figs. 1(d),1(e),1(g), and in other tested materials, see Figs. 2(e)–2(h), show that the required period values to phase-match conical TH generation are readily present in broad distributions of spatial frequencies.

Inscription of nanograting in the volume of nonlinear material and its optical signature (conical TH generation) requires a certain number of consecutive laser pulses (exposure time), which differs in different materials. Even if the same material is used, nanograting formation strongly depends on the input pulse energy and laser repetition rate as well as on specifics of self-focusing and beam filamentation. This is illustrated by an example of sapphire. Figure 6(a) shows the

Optics EXPRESS

number of laser pulses at a repetition rate of 200 kHz needed to inscribe a nanograting in the volume of sapphire crystal, which is justified by the occurrence of conical TH emission in supercontinuum generation experiment as a function of the input pulse energy and peak power. A remarkably long exposure time (almost 8 hours, 5.7×10^9 pulses) for conical TH generation to set in was measured in the absence of filamentation (below supercontinuum generation threshold), with the input pulse energy of 0.71 μJ. Although in this case the beam power exceeds the critical power for self-focusing (P_{cr} = 3.0 MW), the self-focusing distance is greater than the crystal length (6 mm), so the beam experiences just a slight reduction of its diameter and so just a slight increase of the peak fluence with propagation. A dramatic decrease of the exposure time down to ~ 2 min (~ 2.4×10^7 pulses) was measured with the input pulse energy approaching the supercontinuum generation threshold at 1.37 μJ, which in turn indicates formation of a light filament. Thereafter, the exposure time remains nearly constant with further increase of the pulse energy, which we attribute to the intensity clamping effect set by multiphoton absorption and defocusing due to free electron plasma generation.

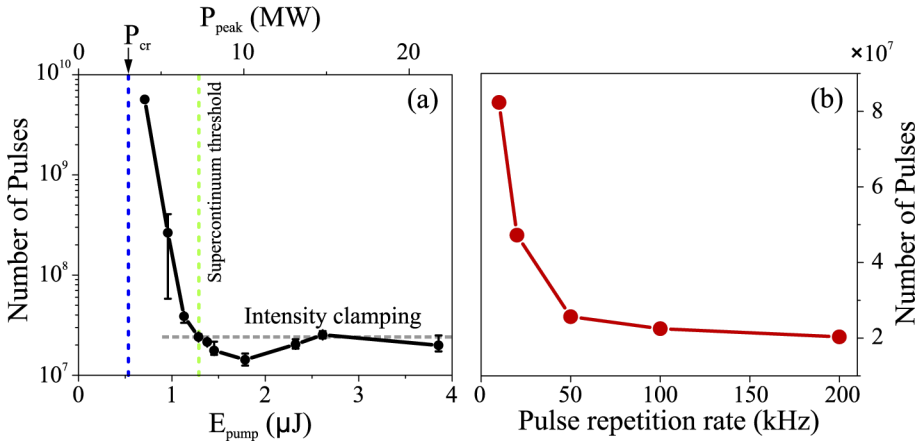

Fig. 6. (a) Number of pulses required to induce conical TH generation versus the input pulse energy and peak power in sapphire (NA=0.051, f=200 kHz). (b) The same as a function of laser repetition rate at a fixed input pulse energy of 2.3 μJ.

Figure 6(b) illustrates the number of pulses required to detect conical TH generation (in fact, to inscribe the nanograting) as a function of laser repetition rate, which was varied from 10 to 200 kHz. The input pulse energy was set at 2.3 μJ, to produce the supercontinuum at the crystal output. An increase of the laser repetition rate reveals a highly nonlinear trend. A rapid drop of the number of pulses required for conical TH generation to occur is observed by increasing pulse repetition rate from 10 to 50 kHz, where the occurrence moment of conical TH emission decreases from ~ 2.3 hours (8.2×10^7 pulses) at 10 kHz to ~ 8.6 min. (2.6×10^7 pulses) at 50 kHz. However, further increase of pulse repetition rate up to 200 kHz shows only a very slight decrease of the number of pulses required to inscribe the nanograting. In the first approximation, the observed trend could be explained with an account of temperature diffusion length, defined as $L = \sqrt{q/f}$, where q is the thermal conductivity and f is the pulse repetition rate. Taking the thermal conductivity of sapphire q = 0.01 cm^2/s [37], a simple calculation yields L = 10 μm at 10 kHz, L = 4.4 μm at 50 kHz and L = 2.2 μm at 200 kHz. Assuming that typical filament diameter in solids is ~ 5 μm [38], the local heat distribution does not dissipate until arrival of successive laser pulse for pulse repetition rates ≥ 50 kHz.

Optics EXPRESS

6. Conclusions

In conclusion, we carried out a detailed study of conical third harmonic generation, which occurs during supercontinuum generation by self-focusing and filamentation of high repetition rate femtosecond pulses from an amplified Yb:KGW laser in various dielectric materials: YAG, sapphire, YLF, LiF, CaF_2, MgF_2, LiSAF, fused silica and BK-7 glass. We show that the observed cone angles of third harmonic emissions in these materials obey noncollinear phase matching condition, which involves reciprocal lattice vector of a nanograting inscribed by a femtosecond filament in the volume of transparent material. Since direct characterization of nanogratings in the volume is technically difficult, the existence of reciprocal lattice vector of the required length to phase match conical third harmonic generation was verified by investigating periodicity features of laser-induced periodic surface structures, where the matter is reorganized in a similar fashion. It was demonstrated that both, high and low spatial frequency laser-induced periodic surface structures possess broad distributions of spatial frequencies (periods) as retrieved by 2D Fourier transform, suggesting that a nanograting with a similar distribution of the periods, including the required period to phase-match conical third harmonic generation is readily produced by femtosecond filament. We believe that our study provides useful insights into the nature of conical third harmonic generation which serves as an optical signature of nanograting formation induced by high repetition rate femtosecond filamentation in transparent dielectric materials.

Funding. Lietuvos Mokslo Taryba (1.2.2- LMT-K-718-02-0017); European Regional Development Fund (1.2.2-LMT-K-718-02-0017).

Acknowledgments. The authors would like to thank Edvinas Skliutas for the access and help with scanning-electron microscopy, Dr. Nail Garejev for the useful digital photography tips and our optician Šarunas Jablonskas for preparing the samples.

Disclosures. The authors declare no conflicts of interest.

Data availability. Data underlying the results presented in this paper are not publicly available at this time but may be obtained from the authors upon reasonable request.

References

1. R. J. Nemanich, D. K. Biegelsen, and W. G. Hawkins, "Aligned, coexisting liquid and solid regions in laser-annealed Si," Phys. Rev. B **27**(12), 7817–7819 (1983).
2. J. Bonse, S. Baudach, J. Krüger, W. Kautek, and M. Lenzner, "Femtosecond laser ablation of silicon–modification thresholds and morphology," Appl. Phys. A **74**(1), 19–25 (2002).
3. H. M. Van Driel, J. E. Sipe, and J. F. Young, "Laser-Induced Periodic Surface Structure on Solids: A Universal Phenomenon," Phys. Rev. Lett. **49**(26), 1955–1958 (1982).
4. J. F. Young, J. S. Preston, H. M. van Driel, and J. E. Sipe, "Laser-induced periodic surface structure. II. Experiments on Ge, Si, Al, and brass," Phys. Rev. B **27**(2), 1155–1172 (1983).
5. J. Bonse, S. V. Kirner, and J. Krüger, "Laser-Induced Periodic Surface Structures (LIPSS)," In *Handbook of Laser Micro- and Nano-Engineering*; K. Sugioka, Ed.; Springer, Cham, Switzerland, 2020), 1–59.
6. J. Bonse, J. Krüger, S. Höhm, and A. Rosenfeld, "Femtosecond laser induced periodic surface structures," J. Laser Appl. **24**(4), 042006 (2012).
7. S. Juodkazis, K. Nishimura, and H. Misawa, "In-bulk and surface structuring of sapphire by femtosecond pulses," Appl. Surf. Sci. **253**(15), 6539–6544 (2007).
8. D. Kim, W. Jang, T. Kim, A. Moon, K.-S. Lim, M. Lee, I.-B. Sohn, and S. Jeong, "Nanostructure and microripple formation on the surface of sapphire with femtosecond laser pulses," J. Appl. Phys. **111**(9), 093518 (2012).
9. K. Miyazaki and G. Miyaji, "Nanograting formation through surface plasmon fields induced by femtosecond laser pulses," J. Appl. Phys. **114**(15), 153108 (2013).
10. G. Eberle, M. Schmidt, F. Pudec, and K. Wegener, "Laser surface and subsurface modification of sapphire using femtosecond pulses," Appl. Surf. Sci. **378**, 504–512 (2016).
11. Y. Ren, L. Zhang, C. Romero, J. R. Vázquez de Aldana, and F. Chen, "Femtosecond laser irradiation on Nd:YAG crystal: Surface ablation and high-spatial-frequency nanograting," Appl. Surf. Sci. **441**, 372–380 (2018).
12. S.-Z. Xu, K. Sun, C.-Z. Yao, H. Liu, X.-X. Miao, Y.-L. Jiang, H.-J. Wang, X.-D. Jiang, X.-D. Yuan, and X.-T. Zu, "Periodic surface structures on dielectrics upon femtosecond laser pulses irradiation," Opt. Express **27**(6), 8983–8993 (2019).
13. S. I. Kudryashov, T. Pflug, N. I. Busleev, M. Olbrich, A. Horn, M. S. Kovalev, and N. G. Stsepuro, "Topological transition from deeply sub- to near-wavelength ripples during multi-shot mid-IR femtosecond laser exposure of a silicon surface," Opt. Mater. Express **11**(1), 1–11 (2021).

Optics EXPRESS

14. R. Buividas, M. Mikutis, and S. Juodkazis, "Surface and bulk structuring of materials by ripples with long and short laser pulses: Recent advances," Prog. Quantum Electron. **38**(3), 119–156 (2014).
15. J. Bonse, S. Höhm, S. V. Kirner, A. Rosenfeld, and J. Krüger, "Laser-induced periodic surface structures - a scientific evergreen," IEEE J. Sel. Top. Quantum Electron. **23**(3), 9000615 (2017).
16. A. S. Alnaser, S. A. Khan, R. A. Ganeev, and E. Stratakis, "Recent advances in femtosecond laser-induced surface structuring for oil-water separation," Appl. Sci. **9**(8), 1554 (2019).
17. J. Bonse, "Quo Vadis LIPSS? - Recent and future trends on laser-induced periodic surface structures," Nanomaterials **10**(10), 1950 (2020).
18. R. Stoian and J.-P. Colombier, "Advances in ultrafast laser structuring of materials at the nanoscale," Nanophotonics **9**(16), 4665–4688 (2020).
19. J. Bonse and S. Gräf, "Maxwell meets Marangoni - a review of theories on laser-induced periodic surface structures," Laser Photonics Rev. **14**(10), 2000215 (2020).
20. Y. Liu, Y. Brelet, Z. He, L. Yu, B. Forestier, Y. Deng, H. Jiang, and A. Houard, "Laser-induced periodic annular surface structures on fused silica surface," Appl. Phys. Lett. **102**(25), 251103 (2013).
21. X. Yu, D. Qi, H. Wang, Y. Zhang, L. Wang, Z. Zhang, S. Dai, X. Shen, P. Zhang, and Y. Xu, "In situ and ex-situ physical scenario of the femtosecond laser-induced periodic surface structures," Opt. Express **27**(7), 10087–10097 (2019).
22. Y. Shimotsuma, P. G. Kazansky, J. Qiu, and K. Hirao, "Self-organized nanogratings in glass irradiated by ultrashort light pulses," Phys. Rev. Lett. **91**(24), 247405 (2003).
23. V. R. Bhardwaj, E. Simova, P. P. Rajeev, C. Hnatovsky, R. S. Taylor, D. M. Rayner, and P. B. Corkum, "Optically produced arrays of planar nanostructures inside fused silica," Phys. Rev. Lett. **96**(5), 057404 (2006).
24. S. Richter, M. Heinrich, S. Döring, A. Tünnermann, and S. Nolte, "Formation of femtosecond laser-induced nanogratings at high repetition rates," Appl. Phys. A **104**(2), 503–507 (2011).
25. S. Richter, M. Heinrich, S. Döring, A. Tünnermann, S. Nolte, and U. Peschel, "Nanogratings in fused silica: Formation, control, and applications," J. Laser Appl. **24**(4), 042008 (2012).
26. M. Beresna, M. Gecevičius, P. G. Kazansky, T. Taylor, and A. V. Kavokin, "Exciton mediated self-organization in glass driven by ultrashort light pulses," Appl. Phys. Lett. **101**(5), 053120 (2012).
27. Y. Liao, J. Ni, L. Qiao, M. Huang, Y. Bellouard, K. Sugioka, and Y. Cheng, "High-fidelity visualization of formation of volume nanogratings in porous glass by femtosecond laser irradiation," Optica **2**(4), 329–334 (2015).
28. E. O. Kissi and Y. Bellouard, "Self-organized nanostructures forming under high-repetition rate femtosecond laser bulk-heating of fused silica," Opt. Express **26**(11), 14024–14037 (2018).
29. A. Rudenko, J.-P. Colombier, and T. E. Itina, "From random inhomogeneities to periodic nanostructures induced in bulk silica by ultrashort laser," Phys. Rev. B **93**(7), 075427 (2016).
30. A. Rudenko, J.-P. Colombier, S. Höhm, A. Rosenfeld, J. Krüger, J. Bonse, and T. E. Itina, "Spontaneous periodic ordering on the surface and in the bulk of dielectrics irradiated by ultrafast laser: a shared electromagnetic origin," Sci. Rep. **7**(1), 12306 (2017).
31. S. Juodkazis, E. Gaizauskas, V. Jarutis, J. Reif, S. Matsuo, and H. Misawa, "Optical third harmonic generation during femtosecond pulse diffraction in a Bragg grating," J. Phys. D: Appl. Phys. **39**(1), 50–53 (2006).
32. L. A. Siiman, J. Lumeau, L. Canioni, and L. B. Glebov, "Non-collinear generation of third harmonic of IR ultrashort laser pulses by PTR glass volume Bragg gratings," Opt. Express **17**(5), 3564–3573 (2009).
33. G. Cheng, K. Mishchik, C. Mauclair, E. Audouard, and R. Stoian, "Ultrafast laser photoinscription of polarization sensitive devices in bulk silica glass," Opt. Express **17**(12), 9515–9525 (2009).
34. Y. Liu, Y. Brelet, Z. He, L. Yu, S. Mitryukovskiy, A. Houard, B. Forestier, A. Couairon, and A. Mysyrowicz, "Ciliary white light: optical aspect of ultrashort laser ablation on transparent dielectrics," Phys. Rev. Lett. **110**(9), 097601 (2013).
35. Q. Liang, Y. Zhong, Z. Fan, H. Diao, V. Jukna, W. Chen, A. Houard, Z. Zeng, R. Li, and Y. Liu, "Optical transmission during mid-infrared femtosecond laser pulses ablation of fused silica," Appl. Surf. Sci. **471**, 506–515 (2019).
36. R. Grigutis, G. Tamošauskas, V. Jukna, A. Risos, and A. Dubietis, "Supercontinuum generation and optical damage of sapphire and YAG at high repetition rates," Opt. Lett. **45**(16), 4507–4510 (2020).
37. E. R. Dobrovinskaya, L. A. Lytvynov, and V. Pishchik, "Properties of Sapphire," In: *Sapphire. Micro- and Opto-Electronic Materials, Structures, and Systems* (Springer, 2009).
38. A. Couairon and A. Mysyrowicz, "Femtosecond filamentation in transparent media," Phys. Rep. **441**(2-4), 47–189 (2007).